remote sensing

MDPI

Article

GNSS-5G Hybrid Positioning Based on Joint Estimation of Multiple Signals in a Highly Dependable Spatio-Temporal Network

Jingrong Liu [1,*], Zhongliang Deng [1], Enwen Hu [1], Yunfei Huang [2], Xiwen Deng [1], Zhichao Zhang [1], Zhenke Ding [1] and Bingxun Liu [1]

[1] School of Electronic Engineering, Beijing University of Posts and Telecommunications, Beijing 100876, China; dengxiwen@bupt.edu.cn (X.D.); 2020110459@bupt.cn (Z.Z.); dingzk@bupt.edu.cn (Z.D.)
[2] China Telecom, Beijing 101399, China; huangyf6.gd@chinatelecom.cn
* Correspondence: jingrongliu@bupt.edu.cn; Tel.: +86-176-1077-8381

Abstract: The Global Navigation Satellite System (GNSS) has been widely used in every area of our daily life to provide accurate Positioning, Navigation, and Timing (PNT) services. However, due to the multipatch effect and an obstructed view of the satellite, GNSS receivers are susceptible to large-ranging errors, which are particularly prevalent in urban areas where precise positioning is indispensable. The deployment of the high-spatial-density Fifth-Generation (5G) network makes it possible to provide a broad area with high-precision positioning service. Obviously, it promoting the deep integration of the GNSS system and the 5G mobile communication network and establishing a Highly Dependable Spatio-temporal Network (HDSN) have become an inevitable trend. The existing algorithm for the fusion of multiple signals has difficulty settling problems such as the fast fluctuation of available signal sources and the poor stability of multi-scale multi-type signal estimation in GNSS-5G hybrid networks. Here, we propose a Square Root Unscented Stable Filter (SRUSF) for GNSS and 5G joint positioning with a compact coupled filter group architecture in a highly dependable spatio-temporal network. A stabilized coefficient is added to guarantee positive covariance of the estimation error. The possibility of divergence of filtering results due to the variation in signal sources and the incomplete agreement between the system model and the actual situation are reduced. The simulation results show that the proposed SRUSF method substantially enhances the positioning accuracy and reliability compared with the other five joint estimation methods for multiple signals. This work will enable the terminal of mass users to provide timing and positioning services with unprecedented accuracy and dependability under the GNSS and 5 G-based spatio-temporal network's architecture.

Keywords: highly dependable spatio-temporal network; GNSS; 5G network; hybrid positioning; estimation method

Citation: Liu, J.; Deng, Z.; Hu, E.; Huang, Y.; Deng, X.; Zhang, Z.; Ding, Z.; Liu, B. GNSS-5G Hybrid Positioning Based on Joint Estimation of Multiple Signals in a Highly Dependable Spatio-Temporal Network. *Remote Sens.* **2023**, *15*, 4220. https://doi.org/10.3390/rs15174220

Academic Editor: Yunbin Yuan

Received: 13 July 2023
Revised: 22 August 2023
Accepted: 23 August 2023
Published: 28 August 2023

1. Introduction

A spatio-temporal network is a strategic symbol of comprehensive national strength, and GNSS and mobile communication networks are important components of the spatio-temporal network system. The global location-based service market size will grow from USD 70.27 billion in 2022 to USD 88.42 billion in 2023, with a compound annual growth rate of 25.8% [1]. The promotion of the deep integration of GNSS system and mobile communication network, the establishment of a new type of ubiquitous, reliable, and integrated location service system platform, and the formation of a highly reliable spatio-temporal network have become an inevitable trend. In recent years, many countries have carried out a major deployment of space-time service systems using GNSS, next-generation mobile communications, and big data to strengthen comprehensive information service capabilities and comprehensively improve the level of the space-time infrastructure's

development. Building a highly dependable spatio-temporal network is urgently needed to solve the problems of network heterogeneity, data-heterogeneity fusion, and trusted positioning under the spatio-temporal network architecture. The scenario of GNSS and 5G hybrid positioning is shown in Figure 1.

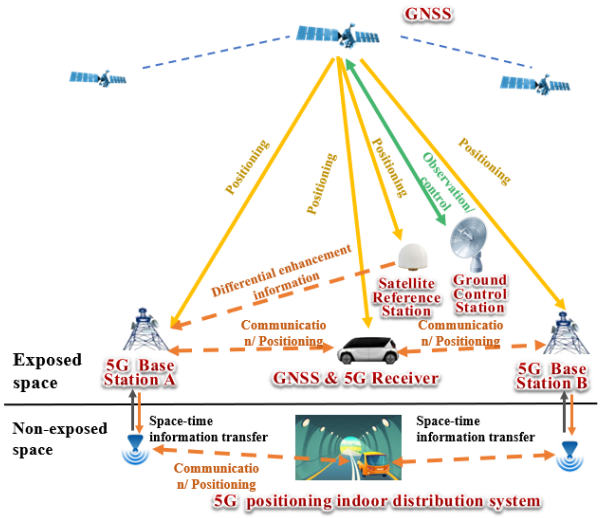

Figure 1. Scenario of GNSS-5G hybrid positioning in a high-dependability spatio-temporal network.

GNSS can provide users with real-time position, speed, and time information. However, with users' increasing requirements with respect to positioning accuracy and robustness, the existing satellite positioning technology can no longer meet the needs of users in the face of complex scenes with high occlusion, high multipath interference effects, and high Non-Line-Of-Sight (NLOS) characteristics such as dense buildings and indoor/outdoor switching [2]. The fusion of GNSS systems with other systems, such as inertial navigation systems [3–5], visual navigation systems [4,5], local sensor networks [6,7], or wireless communication networks [2,8–12], is a feasible option at this time. Numerous scholars have conducted intensive research on this issue. Additional cumulative errors will lead to a decrease in accuracy in the inertial navigation system. The light environment drastically restricts the visual navigation system. Local sensor networks such as Bluetooth and UWB should be deployed independently. The 5G network is a mobile communication system, without the aforementioned deficiencies, that has a high base station density, broad indoor and outdoor coverage, and a wide communication bandwidth. Therefore, it is capable of precisely measuring the relative distance between the base station and the user terminal . The combination of 5G and GNSS signals can effectively address the problems of limited GNSS coverage and poor positioning accuracy in urban canyons.

The GNSS has fully served many key industries, such as national defense and military, mass fields, transportation, public safety, disaster relief and mitigation, agriculture, forestry, animal husbandry and fishery, and urban governance. However, the service is limited or even blocked in indoor, underground, urban canyon, and other sheltered environments. The resources of the 5G mobile communication network are an important supplement to GNSS, and the deep integration of 5G and GNSS is an effective way to realize a ubiquitous and credible spatio-temporal information service. The positioning standards of R16 and R17 have been established in the 5G mobile communication network, and the R18 standard is being studied, which has the potential of sub-meter-level positioning, and its positioning signals can cover indoor and outdoor environments, underground environments, tunnels, urban canyons, and other environments and can become a supplement to the GNSS under a fully occluded environment (indoor, underground, tunnels, etc.), a means of integration and enhancement between a semi-occluded (urban canyons, etc.) and open environment, thus expanding the service scope and scope of GNSS. The GNSS and 5G joint-positioning methods are mainly divided into three types. Firstly, GNSS positioning

results are dominant, and 5G base stations are utilized as communication means to transmit GNSS-enhanced information [13,14]; secondly GNSS positioning signals are blocked or suffer from significant errors, and the positioning result of 5G PRS signal is dominant [11]; thirdly the positioning terminal can receive the GNSS signal and the 5G positioning signal at the same time and can obtain the positioning result through the fusion of the two signals [8–10,12]. Therefore, the fusion positioning algorithm has become a research hotspot [2,12]. The Extended Kalman Filter (EKF)-based algorithm is a widely used filtering algorithm that approximates nonlinear dynamics by linearizing system states and measurements. EKF has been extensively applied in GNSS and multi-sensor integration [15–17]. However, the linearization approximation of EKF for nonlinear systems and noise may lead to the growth of estimation errors. Lu Bai et al. [9] proposed a hybrid sequential-fusion Multiple-Rate Adaptive Kalman Filter (MRAKF) for GNSS-5G hybrid positioning, which is able to adaptively adjust the observation noise covariance matrix. MRAKF can manage the large dynamic range of the measurement noise uncertainty and prevent the decrease in the positioning accuracy. Julier et al. [18] proposed an Unscented Kalman Filter (UKF) as a derivative-free alternative to the extended Kalman filter in the framework of state estimation. Through the utilization of a set of unscented transformation points to represent the mean and covariance of the state distribution, the state of nonlinear systems can be estimated with improved precision. Nevertheless, there is a drawback with filter divergence in the estimation of the state of high-dimensional systems. In GNSS and 5G fusion, the number of observation data is substantial, and the EKF calculation Jacobian matrix is intricate. Many researchers [19–22] have utilized a federated filter algorithm based on the Unscented Kalman Filter to improve the accuracy of low-cost Strapdown Inertial Navigation Systems (SINSs). The Square Root UKF (SRUKF) [23–25] is a modified form of UKF, the filter of which is initialized by calculating the matrix square root of the estimation-error covariance, which is proved to provide a better numerical stability. K. Li. et al. [26] proposed a modified UKF algorithm called a Variational Bayesian-based Unscented Kalman Filter (VBHUKF). Adaptation is achieved by estimating the time-varying observation noise covariance based on Variational Bayesian approximations. The proposed method has better filtering consistency than the standard UKF, and the VBHUKF filter performs better when the observation noise covariance is time-varying and there are outliers in the observation data.

The main contributions of this paper can be summarized as follows. We have proposed a multiple-signal, compact, coupled filter group architecture and a Square Root Unscented Stable Filter algorithm as a solution to the issues in the GNSS-5G hybrid network that the number of available signal sources fluctuates rapidly, the estimation stability of multi-scale and multi-type signals is poor, and dependable positioning is difficult. We have added an additional positive definite parameter to guarantee positive estimation-error covariance. Ultimately, the high-confidence joint positioning of GNSS and 5G is realized, and the divergence of fusion positioning results caused is avoided with abnormal observation data.

The remainder of this paper is organized as follows. Section 2 briefly introduces the GNSS-5G hybrid positioning system model. Section 3 describes the proposed multiple-signal joint estimation method in detail, including a multiple-signal, compact, coupled filter group architecture and the realization of a Square Root Unscented stable filter. In Section 4, the employed simulation settings are explained, the performance of SRUSF in GNSS and 5G Joint Positioning Model is evaluated under different condition, and an analysis of the proposed method is presented. Finally, conclusions are drawn in Section 5.

2. System Model

In this section, the measurement model of the GNSS positioning signal is described, followed by a measurement model of the 5G positioning signal, a clock model of the positioning terminal, and finally, a measurement model of the GNSS and 5G fusion positioning.

2.1. GNSS Receiver Measurement Model

The measurement equation for the m-th satellite is given by

$$y^m_{\mathrm{GNSS}}[t_k] = \tau_{GNSS}[t_k] = h^m_{\mathrm{GNSS}}(\,\mathrm{s}[t_k]) + \omega^m_{\mathrm{GNSS}}[t_k] \tag{1}$$

$$h^m_{\mathrm{GNSS}}(\,\mathrm{s}[t_k]) = \frac{d^m_{GNSS}[t_k]}{c} + \delta[t_k] \tag{2}$$

where m is the satellite number, t_k denotes the measurement time of the receiver, $\tau_{GNSS}[t_k]$ denotes the time delay measurement result, and $h^m_{GNSS}(s[t_k])$ indicates the measurement function that converts the state quantity into the observation quantity, where $\omega[t_k]$ models the uncertainty of the measurement, which is modeled as a zero-mean Gaussian random vector with a covariance of R_{GNSS}. R_{GNSS} is composed of different error sources, including satellite and receiver clock errors, satellite orbit errors, and errors such as ionospheric and tropospheric delays, where c represents the speed of light, $d^m_{GNSS}[t_k]$ indicates the real distance between the terminal and the m-th satellite, and $\delta[t_k]$ denotes the terminal's clock bias in relation to the GNSS satellites. The GNSS measurement results are not available if the GNSS receiver loses its signal under severe multipath effects or when the carrier-to-noise ratio is extremely low. Therefore, in harsh multipath environments such as navigating in a canyon deep within a city, the multipath effect-suppression algorithm must be considered. This article does not discuss the related research on multipath signal modeling or related methods, for which one can refer to [27,28].

2.2. 5G Receiver Measurement Model

Considering the scene of 3D positioning, assuming that the number of line-of-sight 5G base stations is n, the signal-measurement model of the 5G positioning receiver is as follows:

$$\mathrm{y}^n_{5G}[t_k] = [\tau[t_k], \varphi[t_k], \theta[t_k]] = \mathrm{h}^n_{5G}(\,\mathrm{s}[t_k]) + \omega^n_{5G}[t_k] \tag{3}$$

where y represents the collection of measurements; n denotes the number of 5G base stations; t_k indicates the measurement time of the receiver; and τ, φ, and θ represent the measurements of the Time Of Arrival (TOA), azimuth Direction Of Arrival (DOA), and elevation DOA. $s[t_k]$ is the state of the 5G receiver at the timestamp t_k, $\omega[t_k]$ denotes the measurement uncertainty of the receiver, and the nonlinear measurement function $\mathrm{h}^n_{5G}(\,\mathrm{s}[t_k])$ can be expressed as follows:

$$\mathrm{h}^n_{5GUE}(s[t_k]) = \begin{bmatrix} \frac{d^n[t_k]}{c} + \delta[t_k] \\ \arctan\left(\frac{\Delta y^n[t_k]}{\Delta x^K[t_k]}\right) \\ \arctan\left(\frac{\Delta z^n[t_k]}{\sqrt{(\Delta x^n[t_k])^2 + (\Delta y^n[t_k])^2}}\right) \end{bmatrix} \tag{4}$$

where $d^n[t_k] = \sqrt{(\Delta x^n[t_k])^2 + (\Delta y^n[t_k])^2 + (\Delta z^n[t_k])^2}$ indicates the distance from the receiver to the m-th base station and $\Delta x^n[t_k]$, $\Delta y^n[t_k]$, and $\Delta z^n[t_k]$ denote the distance difference between the terminal and the base station in x, y, and z directions, respectively. $\delta[t_k]$ indicates the clock deviation of the terminal relative to the GNSS satellite.

2.3. Receiver Clock Model

For mass-market users, the clock in the positioning receiver usually uses a low-cost consumer crystal oscillator, and its clock deviation relative to the time of the GNSS system is impossible to ignore, which contributes to the clock offset in the terminal being time-varying. Therefore, the clock offset of the terminal must be modeled to represent or estimate the clock offset of the device. Therefore, the clock offset of the receiver must be modeled

to estimate the clock offset of the device. It is shown in [29] that the clock offset of two consecutive adjacent times can be expressed as

$$\rho[t_k] = \rho[t_{k-1}] + \alpha[t_k]\Delta t \tag{5}$$

where Δt represents the time interval between two consecutive measurement times t_{k-1} and t_k, and$\alpha[t_k]$ denotes the clock skew, which is also a time-variable quantity

$$\alpha[t_k] = \omega\alpha[t_{k-1}] + \eta[t_k] \tag{6}$$

where $\eta[t_k] \sim \mathcal{N}\left(0, \sigma_\eta^2\right)$ is additive white Gaussian noise sequence. ω is a coefficient describing the correlation between $\alpha[t_k]$ and $\alpha[t_{k-1}]$. In this paper, ω is set to 1 based on empirical values.

2.4. GNSS and 5G Joint Positioning Model

Aiming to take full advantage of the measurement information offered by GNSS satellites and 5G BSs, we propose a GNSS and 5G fusion positioning model with the input of the observation data of multiple satellites and multiple 5G BSs, which are named GNSS and 5G Joint Positioning Model (GNSS and 5G JPM). The purpose of realizing the fusion positioning of GNSS and 5G is to unify the time-reference and space-reference coordinate system. In this paper, the BDS time and the Earth-Centered Earth-Fixed (ECEF) coordinate system are chosen as the unified benchmarks. Assuming that m satellites and n5G BSs can be observed in each epoch $t_,$ the signal-measurement model of the GNSS and 5G Joint Positioning Receiver (JPR) can be obtained as described in Equation (5):

$$\begin{aligned} y_{\text{GNSS \& 5G}}[t_k] &= \left[\tau^1_{\text{GNSS}}[t_k], \ldots, \tau^m_{GNSS}[t_k], \tau^1_{5G}[t_k], \ldots, \tau^n_{5G}[t_k], \varphi^1[t_k], \theta^1[t_k], \ldots, \varphi^n[t_k], \theta^n[t_k]\right]^T \\ &= h_{\text{GNSS \& 5G}}\left(s_{\text{GNSS \& 5G}}[t_k]\right) + n_{GNSS\&5G}[t_k] \end{aligned} \tag{7}$$

where $\tau^1_{GNSS}[t_k], \ldots, \tau^m_{GNSS}[t_k]$ denotes the TOA JPR obtained from the first to the m-th satellite, $\tau^1_{5G}[t_k], \ldots, \tau^n_{5G}[t_k]$, $\varphi^1[t_k], \theta^1[t_k], \ldots, \varphi^n[t_k]$, and $\theta^n[t_k]$ represent the TOA, azimuth DOA, and elevation DOA of the first to nth 5G base stations received by the JPR, respectively. $h_{GNSS\&5G}$ represents the measurement function of JPM $h_{GNSS\&5G} = \left[h^1_{GNSS}[t_k], \ldots, h^M_{GNSS}[t_k], h^1_{5G}[t_k], \ldots, h^N_{5G}[t_k]\right]^T$, and observation noise is composed of m satellites and n5G base stations $n_{GNSS\&5G}[t_k] = \left[\omega^1_{GNSS}[t_k], \ldots, \omega^m_{GNSS}[t_k], \omega^1_{5G}[t_k], \ldots, \omega^n_{5G}[t_k]\right]^T$.

In the case of synchronized satellites and 5G BSs, the system state of the GNSS and 5G joint 3D positioning can be written as

$$s_{GNSS\&5G}[t_k] = [p[t_k], v[t_k], \rho[t_k], \alpha[t_k]]^T \tag{8}$$

The continuous white noise acceleration model in [9] is used here to characterize the transformation of the JPR's state.

$$s_{GNSS\&5G}[t_k] = \mathbf{F}s_{GNSS\&5G}[t_{k-1}] + \mathrm{u}[t_k] \tag{9}$$

where $\mathbf{F}$ denotes the state-transition matrix, and $\mathrm{u}[t_k]$ is the process noise following a Gaussian distribution.

$$\mathbf{F} = \begin{bmatrix} \mathbf{I}_{3\times3} & \Delta t \cdot \mathbf{I}_{3\times3} & \mathbf{0}_{3\times2} \\ \mathbf{0}_{3\times3} & \mathbf{I}_{3\times3} & \mathbf{0}_{3\times2} \\ \mathbf{0}_{2\times3} & \mathbf{0}_{2\times3} & \mathbf{F}_{\text{Clock}} \end{bmatrix}, \mathbf{F}_{\text{Clock}} = \begin{bmatrix} 1 & \Delta t \\ 0 & \omega \end{bmatrix} \tag{10}$$

The four elements at the top-left corner of matrix **F** represent the constant-velocity (CV) model, and Δt is the interval between two adjacent epochs. $\mathbf{F}_{\text{Clock}}$ describes the JPR clock model obtained from [29].

$$\mathbf{Q} = \begin{bmatrix} \frac{\sigma_v^2 \Delta t^3}{3} \cdot \mathbf{I}_{3\times3} & \frac{\sigma_v^2 \Delta t^2}{2} \cdot \mathbf{I}_{3\times3} & \mathbf{0}_{3\times1} & \mathbf{0}_{3\times1} \\ \frac{\sigma_v^2 \Delta t^2}{2} \cdot \mathbf{I}_{3\times3} & \sigma_v^2 \Delta t \cdot \mathbf{I}_{3\times3} & \mathbf{0}_{3\times1} & \mathbf{0}_{3\times1} \\ \mathbf{0}_{1\times3} & \mathbf{0}_{1\times3} & \frac{\sigma_\eta^2 \Delta t^3}{3} & \frac{\sigma_\eta^2 \Delta t^2}{2} \\ \mathbf{0}_{1\times3} & \mathbf{0}_{1\times3} & \frac{\sigma_\eta^2 \Delta t^2}{2} & \sigma_\eta^2 \Delta t \end{bmatrix} \tag{11}$$

where σ_v and σ_η denote the variances of the JPR velocity and clock skew in [29], respectively.

3. The Proposed Multiple-Signal Joint Estimation Method

3.1. Multiple-Signal Compact Coupled Filter Group Architecture

The currently widely used multi-signal source-fusion method adopts a cascaded filter architecture. After the individual positioning results of each sensor are given, the positioning settlement results are fused according to a certain weighted algorithm. These types of methods process the observations according to the time sequence according to the sequential fusion strategy and only need to fuse and estimate the independent positioning results. The advantage of this fusion method is that the structure is flexible and the implementation complexity is low. However, the disadvantages of this type of method are also obvious. Ignoring a large amount of prior information may lead to a significant decrease in the accuracy of the estimation results. In order to entirely achieve joint estimation and high-precision measurement of GNSS and 5G signals, this paper proposes a tightly coupled filter group, whose architecture is shown in Figure 2. This method first filters the observations of each channel of the GNSS and 5G joint positioning terminal separately in the first group, and then fuses the observations of each signal source to give the optimal estimate of the GNSS and 5G joint positioning results in the second group. In the first group, UKF algorithm is utilized to predict GNSS observation and 5G observation respectively. In the second group, we adopt the Square Root Unscented stable filter algorithm proposed in next section, multiple GNSS and 5G measurement obtained from the first group are efficiently fused into the position estimation to ensure the high dependability positioning.

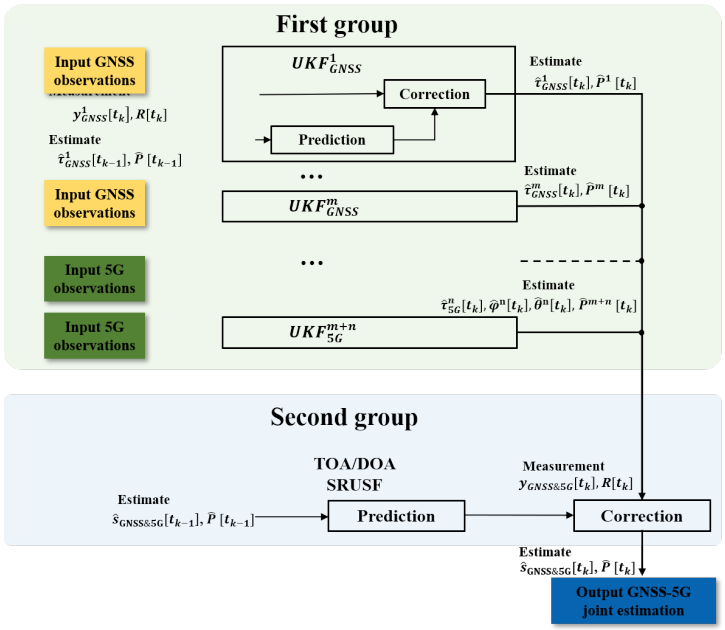

Figure 2. GNSS and 5G joint positioning compact coupled filter group architecture.

The first group utilizes UKF to estimate the observation of 5G and GNSS, a general algorithm of UKF can be founded in [18] and the state equation of the system can be expressed as

$$\begin{aligned} \boldsymbol{s}_{\mathrm{GNSS\&5G}}[t_k] = [&\tau_{GNSS}[t_k], \tau_{5GBS}[t_k], \varphi_{5GBS}[t_k], \theta_{5GBS}[t_k] \\ &\Delta\tau_{GNSS}[t_k], \Delta\tau_{5GBS}[t_k], \Delta\varphi_{5GBS}[t_k], \Delta\theta_{5GBS}[t_k]]^T \end{aligned} \tag{12}$$

where $\tau_{GNSS}[t_k], \tau_{5GBS}[t_k], \varphi_{5GBS}[t_k], \theta_{5GBS}[t_k]$ denote GNSS TOA, 5G TOA, azimuth angle and elevation angle, respectively. Furthermore, parameters $\Delta\tau_{GNSS}[t_k], \Delta\tau_{5GBS}[t_k], \Delta\varphi_{5GBS}[t_k]$, $\Delta\theta_{5GBS}[t_k]$ denote the rate of change of the corresponding variables.

In GNSS and 5G fusion positioning scenarios, there often exist a large number of NLOS channels, and the positioning results of direct integration of multiple signal sources may result in an unacceptable rise in location error. At present, the widely used NLOS error suppression methods are mainly divided into error compensation based on NLOS error distribution model and suppression methods based on observation screening.

Due to the wide coverage of the spatio-temporal network composed of GNSS and 5G communication networks, the modeling complexity and cost of collecting NLOS errors are extremely high. In the method proposed in this paper, UKF is used in the first group to predict and update the observation and the change rate of 5G and GNSS, respectively, which provides the feasibility for using signal quality evaluation and observation screening algorithm to exclude the NLOS channel observation information and can prevent excessive NLOS errors from being introduced into the joint positioning results of the second group.

The second group utilizes the SRUSF algorithm introduced in Section 3.2 to estimate the receiver's position, velocity, clock offset, and clock skew. The state equation can be expressed as

$$\boldsymbol{s}_{\mathrm{GNSS\&5G}}[t_k] = \left[\mathbf{p}^{\mathrm{T}}[t_k], \mathbf{v}^{\mathrm{T}}[t_k], \rho[t_k], \alpha[t_k]\right]^{\mathrm{T}} \tag{13}$$

In the GNSS and 5G joint positioning compact-coupled-filter group architecture, each filter in the first group outputs updated and filtered GNSS and 5G observations into the second group, which are used to modify the measurements of each channel in the receiver at the current time. By combining the estimated value of the previous time, the second group uses the SRURF algorithm to solve the fusion of multiple signal sources' TOA and DOA and gives the joint estimation of the position, speed, and clock offset of the positioning terminal with GNSS and 5G.

3.2. Square Root Unscented Stable Filter

In order to enhance the numerical stability of UKF, the square root form of the state covariance is introduced. In the Square Root Unscented stable filter implementation, the square root of the state covariance is propagated directly, avoiding the requirement to refactorize the covariance at each iteration. In addition, the square root form has the additional advantages of numerical stability and positive semi-certainty of the state covariance. During the fusion of GNSS and 5G observations, the stability of the filter must be guaranteed. Therefore, a stability factor is added as a slight modification to ensure the reliability of the SRUSF.

Unscented Transformation is introduced in SRUSF, utilizing the deterministic "sampling" method to calculate the mean and covariance terms. The relative locations of the sampling points and their corresponding weights are based on the following basic principle: they can capture the most important statistical properties of the prior random variables. $2\,\mathrm{L}+1$ sigma points are selected according to the square root decomposition of a priori covariance. The nonlinear function is applied to each sigma point to yield a cloud of transformed points, and the estimate of the nonlinearly transformed mean and covariance can be obtained by weighting the transformed points. The initial system state $\boldsymbol{s}_{\mathrm{GNSS\&5G}}[t_0] \sim \mathcal{N}(\mathrm{m}, \mathrm{P})$ follows a Gaussian distribution with mean m and variance P.

From the column of system state matrix $s_{\mathrm{GNSS\&5G}}[t_k]$ we can obtain 2 L + 1 sigma points

$$\begin{cases} x_0 = m \\ x_i = m + (\sqrt{(L+\lambda)\mathbf{P}})_i \quad i = 1, \ldots, L \\ x_i = m - (\sqrt{(L+\lambda)\mathbf{P}})_{i-L} \quad i = L+1, \ldots, 2L \end{cases} \tag{14}$$

Calculating the corresponding weight for each sigma point,

$$W_0^{(m)} = \frac{\lambda}{(L+\lambda)} \tag{15}$$

$$W_0^{(c)} = \frac{\lambda}{(L+\lambda) + (1 - \alpha^2 + \beta)} \tag{16}$$

$$W_i^{(m)} = W_i^{(c)} = \frac{1}{2(L+\lambda)}, i = 1, \ldots, 2L \tag{17}$$

where the scaling parameter can be expressed as $\lambda = \alpha^2(L + \kappa) - L$. L is the dimension of the state space matrix, and α and κ determine the distribution of sigma points near the mean value. The parameter α is typically set to a smaller positive value $1 \times 10^{-4} \leq \alpha \leq 1$ [30]; κ is a secondary scaling parameter, which is often set to 0; and β is a scalar parameter used to incorporate prior information on probability distributions over the state space of the system. For A Gaussian distribution, $\beta = 2$ is optimal.

These sigma vectors are propagated through the nonlinear function

$$y_i = h(x_i) i = 0, \ldots \tag{18}$$

The covariance of the GNSS-5G joint-positioning state-prediction error can be expressed as

$$P^-[t_k] = FP[t_k]F^T + Q[t_k] \tag{19}$$

where $P[t_k]$ denotes the estimation-error covariance and its square root form $R[t_k]$ is presented in (20), and $Q[t_k]$ is the Gaussian process noise matrix at t_k.

$$P[t_k] = R[t_k](R[t_k])^T \tag{20}$$

By introducing the QR decomposition, the square root of the state prediction covariance can be expressed as

$$R^-[t_k] = \left(\mathrm{qr}\left\{ \left[FR[t_k] \sqrt{Q[t_k}} \right]^T \right\} \right)^T \tag{21}$$

where the "qr" (orthogonal triangular decomposition) is a MATLAB function that denotes the QR decomposition.

In the GNSS and 5G joint positioning SR-USF algorithm, the process noise consists of two parts, the deterministic noise and the stochastic noise. The deterministic noise can be settled using a priori knowledge, while the stochastic noise attributed to the modeling error should be compensated accurately. Because of this modeling inaccuracy, the innovation's expected mean and covariance could be divergent from their actual values in practice. A stabilized coefficient is proposed here to solve this problem, which will undoubtedly improve the competitiveness of this method.

$$R[t_k] = \sqrt{\varphi[t_k]} R^-[t_k] \tag{22}$$

The estimated innovation covariance $P_{\gamma,\gamma}[t_k]$ should be larger than or equal to the real one $\mathrm{E}\{\gamma[t_k]\gamma^T[t_k]\}$ so as to maintain consistent estimates.

$$P_{\gamma,\gamma}[t_k] \geq \mathrm{E}\Big\{\gamma[t_k]\gamma^T[t_k]\Big\} \tag{23}$$

$$\gamma[t_k] = y[t_k] - \hat{y}[t_k] \tag{24}$$

where $\gamma[t_k]$ is the innovation sequence and $\hat{y}[t_k]$ is the predicted measurement. It is significant to point out that the innovation covariance can be written as

$$P_{\gamma,Y}[t_k] = H[t_k]P[t_k]H^T[t_k] + Q[t_k] \tag{25}$$

where $P[t_k]$ is the covariance of the predicted state and the cross-covariance between the measurements, and the predicted state is denoted by $P_{x,y}[t_k]$:

$$P_{x,z}[t_k] = P[t_k]H^T[t_k] \tag{26}$$

Combining Equations (25) and (26) leads to Equation (27)

$$P_{\gamma,\gamma}[t_k] = P_{x,y}^T[t_k]P^{-1}[t_k]P_{x,y}[t_k] + Q[t_k] \tag{27}$$

Incorporating across Equations (23) to (27) yields Equation (28), the fading factor introduced into the predicted state covariance should meet the requirements

$$\varphi[t_k] \geq \frac{E\{y[t_k]y^T[t_k] - Q[t_k]}{\left(P_{x,y}^-[t_k]\right)^T(P^-[t_k])^{-1}P_{x,y}^-[t_k]} \tag{28}$$

where $P^-[t_k]$ is the covariance of the predicted state $P[t_k] = \varphi[t_k]P^-[t_k]$, and$P_{x,y}^-[t_k]$ is the cross-covariance of the state and measurement without the fading factor $P_{x,y}[t_k] = \varphi[t_k]P_{x,y}^-[t_k]$.

Consequently, it can be verified that the lower bound of the stabilized coefficient $\varphi[t_k]$ obtained in Equation (28) can be used to mitigate the modeling error by preserving the estimation consistency of the innovation. The square root of the predicted measurement covariance can be derived according to Equation (21)

$$R_{y,y}[t_k] = \left(\mathrm{qr}\left\{\begin{bmatrix} y^*[t_k] & \sqrt{U[t_k}\end{bmatrix}\right\}^T\right)^T \tag{29}$$

$$y^*[t_k] = [(y[t_k])_0 - \hat{y}[t_k] \cdots (y[t_k])_i - \hat{y}[t_k] \cdots (y[t_k])_{2L} - \hat{y}[t_k]] \times \mathrm{diag}\left(\sqrt{W^{(c)}}\right) \tag{30}$$

where L is the dimension of the receiver. $(y[t_k])_i, i = 0, 1, \ldots, 2L$ is the propagated sigma point, and $y[t_k]$ is the predicted measurement results. $U[t_k]$ is the Gaussian measurement noise matrix at t_k.$\sqrt{W^{(c)}}$ denotes the weight of the sigma points. The state covariance derived from QR decomposition can be calculated using

$$R[t_k] = \left(\mathrm{qr}\left\{\left[\chi^*[t_k] - y^*[t_k] \quad K[t_k]\sqrt{U[t_k]}\right]^T\right\}\right)^T \tag{31}$$

$$\chi^*[t_k] = \left[(\chi[t_k])_0 - \hat{s}[t_k] \cdots (\chi[t_k])_i - \hat{s}[t_k] \cdots (\chi[t_k])_{2n_x} - \hat{s}[t_k]\right] \times \mathrm{diag}\left(\sqrt{W^{(c)}}\right) \tag{32}$$

where $(\chi[t_k])_i, i = 0, 1, \ldots, 2L$ denotes the propagated sigma points and $K[t_k]$ is the filtering gain.

The SR-USF algorithm based on the QR decomposition for the GNSS and 5G joint positioning over the k sampling period is summed up in the Algorithm 1 in detail.

Algorithm 1: SRUSF for the GNSS and 5G joint positioning

Initialization Denote the estimated state of GNSS and 5G joint positioning and its square root of the prediction error covariance at t_k^i by $\hat{s}_{\mathrm{GNSS\&5G}}[t_k]$ and $R[t_k]$.

For every iteration k=1, …, T

(1) The prior estimate for predicting the state of the system and the square root of its covariance are as follows

$$\hat{s}_{\mathrm{GNSS\&5G}}[t_k] = F\hat{s}_{\mathrm{GNSS\&5G}}[t_{k-1}] \tag{33}$$

$$R^-[t_k] = \left(\mathrm{qr}\left\{\left[FR[t_k]\sqrt{Q[t_k]}\right]^T\right\}\right)^T \tag{34}$$

(2) Generate 2L+1 sigma points

$$\begin{aligned}\chi^{-(0)}[t_k] &= \hat{s}^-_{\mathrm{GNSS\&5G}}[t_k]\\ \chi^{-(i)}[t_k] &= \hat{s}^-_{\mathrm{GNSS\&5G}}[t_k] + \sqrt{\lambda+L}\left(R^-[t_k]\right)_i\\ \chi^{-(L+i)}[t_k] &= \hat{s}^-_{\mathrm{GNSS\&5G}}[t_k] - \sqrt{\lambda+L}\left(R^-[t_k]\right)_i\end{aligned} \tag{35}$$

where i = 1,…,L

(3) Propagate the sigma points in GNSS-5G joint positioning model

$$y^{-(i)}[t_k] = h_{GNSS\&5G}\left(\chi^{-(i)}[t_k]\right) i = 0, 1, \ldots, 2L \tag{36}$$

(4) Evaluate the predicted value of the measurement result

$$\hat{y}^-[t_k] = \sum_{i=0}^{2L} W_i^{(m)}\left(y^-[t_k]\right)_i \tag{37}$$

where $W_i^{(m)}$ is the mean weights of the sigma points.

(5) Compute the innovation

$$\gamma^-[t_k] = y[t_k] - \hat{y}^-[t_k] \tag{38}$$

(6) Calculate the cross covariance

$$P^-_{x,y}[t_k] = \sum_{i=0}^{2L} W_i^{(c)}\left(\left(\chi^-[t_k]\right)_i - \hat{s}^-[t_k]\right) \times \left(\left(y^-[t_k]\right)_i - \hat{y}^-[t_k]\right) \tag{39}$$

(7) Establish a stabilized coefficient and introduce it into the square root covariance of state prediction.

$$R[t_k] = \sqrt{\varphi[t_k]}R^-[t_k] \tag{40}$$

(8) Generate the new sigma points using the newly predicted state and execute step 2 to step 6 to repeatedlygenerate new innovation and the cross covariance.

(9) Calculate the square root of the innovation covariance

$$R_{y,y}[t_k] = \left(\mathrm{qr}\left\{\begin{bmatrix} y^*[t_k] & \sqrt{U[t_k]}\end{bmatrix}^T\right\}\right)^T \tag{41}$$

(10) Calculate the Kalman gain and update the GNSS and 5G estimate state

$$K[t_k] = \left(P_{x,y}[t_k]/R_{y,y}[t_k]\right)/R^T_{y,y}[t_k] \tag{42}$$

$$\hat{s}[t_k] = \hat{s}^-[t_k] + K[t_k]\gamma[t_k] \tag{43}$$

$$R[t_k] = \left(\mathrm{qr}\left\{\left[\chi^*[t_k] - K[t_k]y^*[t_k] \quad K[t_k]\sqrt{U[t_k]}\right]^T\right\}\right)^T \tag{44}$$

End

4. Simulation Results and Analysis

In this section, the performance of SRUSF in GNSS and the 5G joint positioning model is evaluated regarding measurements' estimation error and positioning error under different conditions. Section 4.1 describes the setup of the simulation scenario and the simulation parameters, and in Section 4.2, we validate the advantages of the proposed SRUSF algorithm. MATLAB 2022a is used to process the data, and the computer configuration is as follows: Intel i5-10400H (CPU), 24 GB (RAM), and Windows 10 (64 bit).

4.1. Parameter Settings

Both pseudorange measurements from GNSS and TOA/AOA measurements from 5G BSs are fused for positioning. Some important simulation parameters for GNSS and 5G BSs are summarized in Table 1. The transmit signal is the 5G positioning reference signal (PRS) conforming to 3GPP TS38.211 [31]. The time of the GNSS and 5G network can be synchronized precisely according to [32].

Table 1. Parameters.

Parameters	Value
5G carrier frequency	3.5 GHz
5G bandwidth	100 MHz
Subcarrier spacing	30 KHz
Total number of satellites	10
Total number of 5G BSs	10

The simulation lasts for a total of 1000 s. The update rates of the GNSS and 5G PRS are set to 1 HZ. The GNSS-5G joint positioning receiver moves straight ahead in the x-direction at 2 m/s. The STD of the clock skew noise σ_ε is set to 1 ns. Only the line-of-sight conditions are simulated since the NLOS-suppression and observation-screening functions are not included.

4.2. Performance Evaluation

We evaluate the horizontal localization accuracy of the proposed hybrid positioning method over different simulation scenarios and compare it with seven state-of-the-art methods, including the standard EKF, MRAKF, UKF, SRUKF, VBHUKF, and SRUSF, to verify its performance. Only 2D scenarios are considered here, but the extension to 3D is quite straightforward.

(1) Positioning performance of the multiple-signal joint estimation method

The positioning error and the cumulative distribution function (CDF) of the proposed method are compared with those of the other five methods. From Figures 3 and 4, we can conclude that among the six observation fusion methods for GNSS and 5G joint positioning, the positioning algorithm based on the EKF filtering has the largest horizontal positioning error, and the horizontal positioning error is 1.98 m in 90% of cases. This is probably because the EKF in the system model uses the Jacobian matrix to calculate the observation matrix, which will bring a certain degree of precision loss. This could be due to the fact that the EKF must derive the Jacobian matrix to obtain the observation matrix, which will bring a certain degree of precision loss. Compared with EKF, the RMSE of MRAKF is reduced by more than 0.4 m on average, indicating the superiority of adaptive strategy filtering. UKF utilizes the UT transform to avoid the accuracy loss caused by nonlinear problems, and its performance is significantly better than standard EKF. In 90% of cases, the horizontal positioning error is 1.55 m. VBHUKF uses the variable Bayesian approximation to estimate the covariance of time-varying measurement noise to achieve self-adaptation. Compared with UKF, it has better filtering consistency, and the positioning accuracy is about 10% higher than that of UKF. SRUKF introduces the square root form of covariance into UKF

to ensure the semi-positive qualitative value of the state space covariance matrix, and the output numerical results are more stable. The proposed SRUSF is superior to the five other filtering methods, the positioning accuracy is slightly better than that of SRUKF and significantly better than other methods, and the positioning error of 0.97 m is achieved in 90% of cases. This is mainly due to the fact we have innovatively proposed a tight-coupled filter group. First, the observations of the GNSS and 5G joint positioning receiver are filtered independently, and then the observations of each signal source are fused to provide an optimal positioning estimate. The stabilized coefficient is introduced in the updating process of the state prediction covariance at the same time, which will undoubtedly reduce the possibility of the divergence of the filtering results due to the imperfect match between the system model and the actual situation and ultimately improve the positioning accuracy of the algorithm.

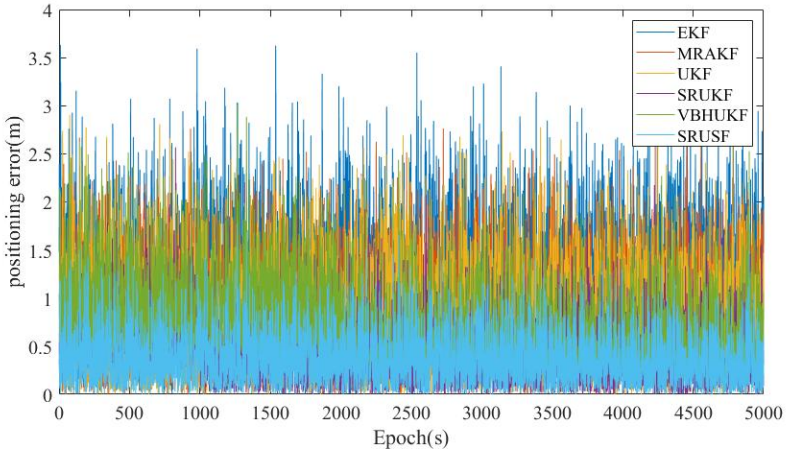

Figure 3. Positioning error comparison of EKF, MRAKF, UKF, SRUKF, VBHUKF, and the proposed SRUSF method.

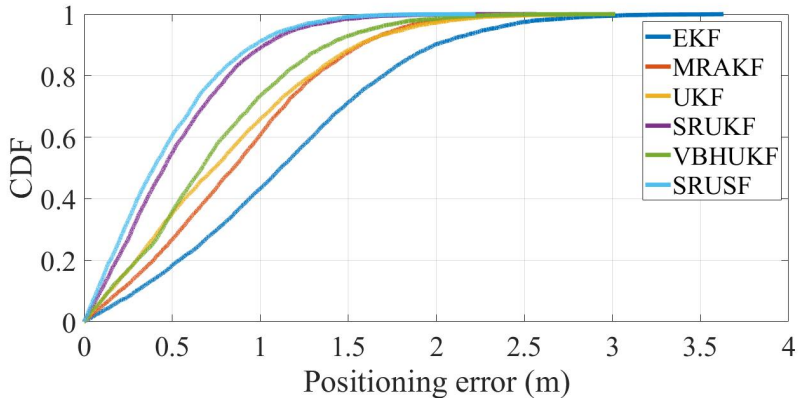

Figure 4. CDF of positioning error for EKF, MRAKF, UKF, SRUKF, VBHUKF, and the proposed SRUSF method.

(2) Positioning performance with different numbers of available signal sources

The positioning error of the GNSS-5G joint positioning system is closely related to the following factors: the modeling accuracy of the system model, the measurement error, the signal propagation error, the geometry of the signal source, the number of visible signal sources, and the positioning algorithm. The first three items are related to system design parameters and the baseband signal processing algorithm and are not within the scope of this paper. The geometry distribution of signal sources also has an important impact on positioning errors. However, under ideal conditions when the signal sources are evenly distributed, the impact on positioning errors is relatively small. This paper mainly focuses

on the relationship between the number of positioning signals received and the positioning accuracy in the GNSS and 5G joint positioning system, as well as the influence of different fusion positioning algorithms on the results. Figure 5 presents the relationship between the positioning RMSE in the horizontal planes and the number of positioning signals.

It can be seen that when the number of positioning signals received by the receiver increases from 3 to 10, the positioning errors of each fusion algorithm are significantly reduced. When the number of available positioning signals is further increased, the positioning accuracy is not greatly improved. Compared with the methods EKF, MRAKF, UKF, SRUKF, VBHUKF, and SRUSF, the performance of the proposed SRUSF algorithm is close to that of other methods, but the performance of the SRUSF algorithm is still better than the other methods, showing high numerical stability.

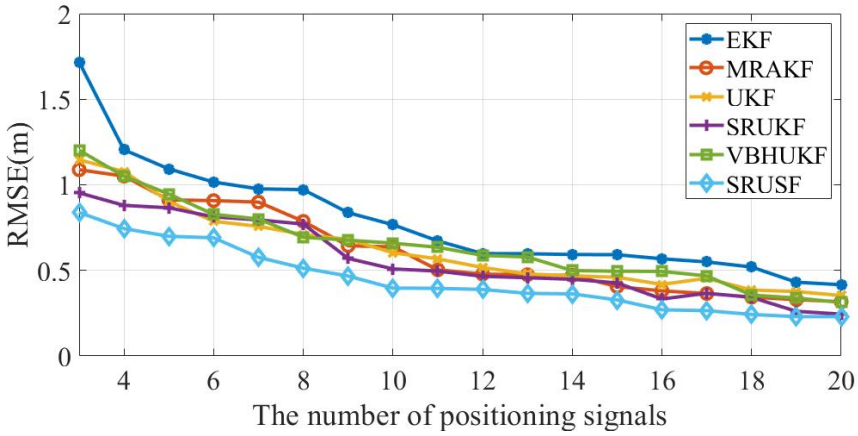

Figure 5. Positioning RMSE versus the number of positioning signals with different methods.

(3) GNSS and 5G joint positioning performance in a typical environment

In order to further prove the superiority of the SRUSF algorithm proposed in this paper, three typical GNSS and 5G joint positioning scenarios are considered in this section, including the slight occlusion of satellite signals, the moderate occlusion of satellite signals, and the severe occlusion of satellite signals. We simulate different numbers of visible satellites and present the performance of various positioning algorithms in different environments. The 5G positioning base station can be arranged according to the requirements, assuming that the 5G base station is evenly distributed around the positioning receiver. An excessive number of base stations is not conducive to observing the impact of changes in the number of GNSS satellites on the positioning accuracy, so the number of 5G positioning base stations is set to four. We generate three sets of observation data with different accuracy levels, and the mean of the real positioning results is set to 0, and STDs are set to 0.5, 0.4, and 0.3 m. In the three typical scenarios, the sky plot and the Taylor diagram are given.

In the sky plot, the blue circle represents the GNSS satellite, the number in the middle represents the satellite number, the purple hexagram represents the 5G positioning base station, and the number in the middle represents the base station number. The rings from the outside to the inside represent different elevation angles, ranging from 0 to 90 degrees, and the numbers on the outside of the outermost circle represent azimuth angles, ranging from 0 to 360 degrees. In the Taylor diagram, the red axis represents the STD of the positioning result, the green dashed line represents the RMSE of the positioning result, and the blue axis represents the correlation coefficient of the output result. Figure 6 shows the scene in which GNSS signals are slightly blocked. The geometric distribution of satellites is good, 10 GNSS satellites can be seen, the elevation distribution is between 10° and 80°, and four 5G positioning base stations can be seen. The EKF algorithm performs the worst, and the STD and RMSE of the output results of MRAKF, UKF, SRUKF, VBHUKF, and SRUSF are very close to each other. The SRUSF proposed in this paper is about 7% higher than the

suboptimal SRUKF algorithm, and the data consistency of SRUKF and SRUSF is obviously better than that of other methods.

Figure 7 shows a scene in which GNSS signals are moderately obstructed, such as the entrance of a tunnel or the side of a tall building. The geometric distribution of satellites is poor, and six GNSS satellites can be seen. The RMSE of EKF, MRAKF, UKF, SRUKF, VBHUKF, and SRUSF deteriorated significantly compared with what is shown in Figure 6, but the increase in RMSE in SRUSF proposed in this paper is the least, which is 18% lower than the suboptimal SRUKF algorithm. In addition, it can be seen that the correlation coefficient of SRUSF is significantly higher than other methods, which reflects the advantage of adding a stabilized coefficient in the state prediction covariance during the updating process.

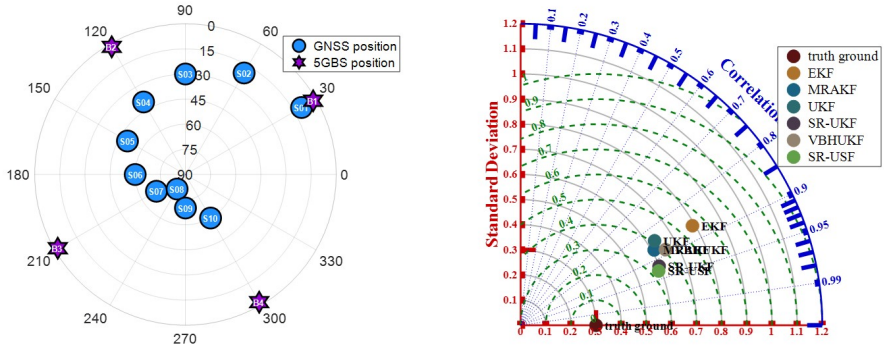

(**a**) Sky plot (**b**) Taylor diagram

Figure 6. GNSS-5G hybrid positioning with slight occlusion. (**a**) Sky plot (**b**) Taylor diagram.

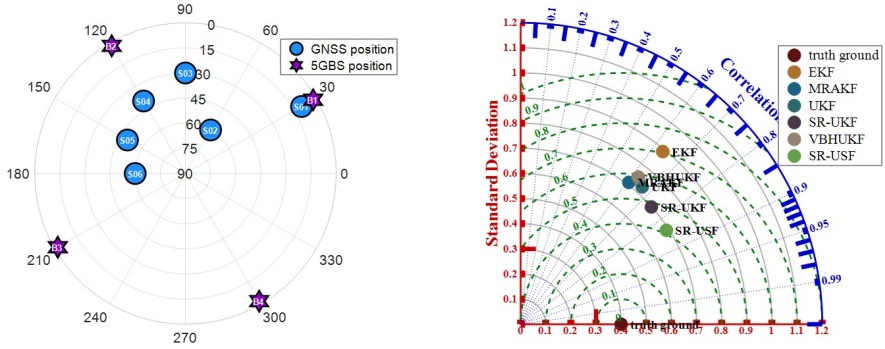

(**a**) Sky plot (**b**) Taylor diagram

Figure 7. GNSS-5G hybrid positioning with moderate occlusion. (**a**) Sky plot (**b**) Taylor diagram.

Figure 8 shows a scene where GNSS signals are severely blocked, such as an urban canyon or an indoor environment. Only two GNSS satellites can be seen, and elevation is distributed between 10° and 30°. The RMSE of EKF, MRAKF, UKF, SRUKF VBHUKF, and SRUSF is significantly larger than that in Figure 7 and the correlation coefficient sharply is reduced as well. However, the proposed SRUSF remains the optimal algorithm and is about 9% better than the suboptimal SRUKF algorithm.

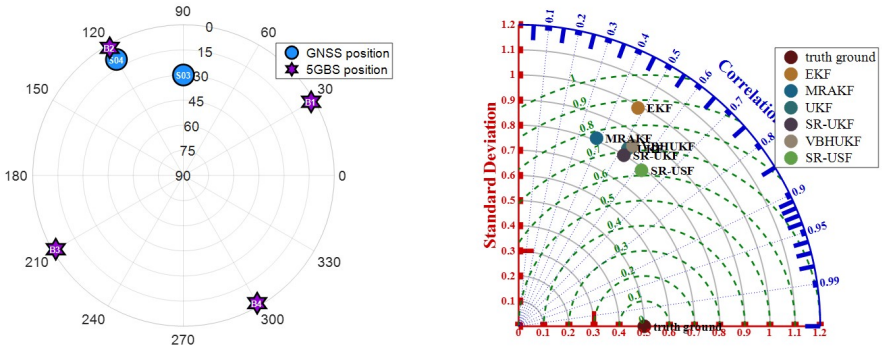

(**a**) Sky plot (**b**) Taylor diagram

Figure 8. GNSS-5G hybrid positioning with severe occlusion. (**a**) Sky plot (**b**) Taylor diagram.

As can be seen in Figures 6–8, the SRUSF algorithm proposed in this paper outperforms other methods in all three typical scenarios: slight occlusion, moderate occlusion, and severe occlusion of satellite signals. In the scenario with slight occlusion, the performance of each positioning algorithm is close because of the sufficient number of visible signal sources. The SRUSF algorithm has the most obvious advantage in the scene with moderate occlusion, and the RMSE of the output is about 18% higher than that of the suboptimal SRUKF algorithm, and the data correlation coefficient is also the largest. In the scene with severe occlusion, the RMSE of each algorithm increases significantly, and the correlation coefficient decreases at the same time, but the performance of the SRUSF algorithm is still superior to that of the other algorithms. On the whole, the output results of SRUSF based on the square root of covariance are more stable. SRUSF innovatively introduces the stabilized coefficient to predict the covariance matrix of the error, which further prevents the divergence of filtering results and increases the dependability of the output. The multiple-signal joint estimation method based on SRUSF algorithm is more suitable for GNSS and 5G hybrid positioning because of the more reliable and dependable state estimation results.

5. Discussion

The potential real-world applications of this article can be divided into the following three aspects. Firstly, enhanced localization and tracking: this research can be widely applied to scenarios requiring high-precision positioning. Through the integration of 5G New Radio (NR) Release 17 and GNSS, a positioning accuracy of 0.2 m can be achieved in indoor and outdoor environments, which will provide essential support for human activity trajectory recognition and robot navigation. Secondly, smart manufacturing: the integration of 5G and GNSS will offer paramount advantages in smart factory scenarios. This could enable factory nodes and robots to seamlessly navigate, coordinate, and map the environment, which is conducive to fulfilling the demand of ultra-reliability, ultra-low latency, and massive connectivity often encountered in smart factory scenarios. Finally, vehicle-to-everything (V2X): autonomous vehicles are expected to fundamentally change the transportation industry, increasing highway capacity and traffic flow and hopefully reducing accidents. The integration of 5G and GNSS could provide environmental information to support fast vehicle platooning, secure and seamless access, and simultaneous localization and mapping.

In this paper, a multiple-signal joint estimation method for GNSS-5G hybrid positioning in a highly dependable spatio-temporal network is proposed. A multiple-signal compact coupled filter group architecture is presented to fuse the measurements of GNSS and 5G. This filter group first filters the observations of each channel of the GNSS-5G joint positioning terminal separately and then fuses the observations of each signal source to give the optimal estimate of the GNSS-5G joint positioning results. Furthermore, a Square Root Unscented stable filter is proposed to guarantee positive estimation-error covariance and avoid the divergence of fusion positioning results caused by abnormal observation data

since the square root of the covariance with stabilized coefficient rather than the covariance itself propagates. Finally, comprehensive simulations are carried out to evaluate regarding the measurements' estimation error and positioning error under different conditions. It is obvious that the proposed SRUSF method substantially enhances the positioning accuracy and reliability compared with the five multiple-signal joint estimation methods. Especially in the scene with moderate occlusion, the RMSE of SRUSF is 18% higher than that of the suboptimal algorithm.

6. Conclusions

In this study, we sought to provide a GNSS and 5G signal joint processing method in support of the general applicability of a highly dependable spatio-temporal network. The proposed approach exhibits considerable promise for multiple-signal joint estimation. This paper will provide significant assistance for highly dependable PNT services for mass users under the GNSS-and-5G-based spatio-temporal network architecture. In the future, we will start from the mass-scale application of the integration of the GNSS and 5G mobile communication network, considering the credibility of positioning results provided via the novel spatio-temporal network, to further improve the precision, availability, and dependability of the PNT service. However, a field test still needs to be carried out in the actual environment in the future. In addition, although the errors caused by multi-type and multi-scale signal switching are considered in this paper, more complex error models and suppression methods can be studied in the future to further improve the receiver's robustness to unknown errors.

Author Contributions: Conceptualization, Z.D. (Zhongliang Deng) and Y.H.; methodology, J.L. and E.H.; software, J.L.; validation, J.L., X.D., Z.Z., Z.D. (Zhenke Ding) and E.H.; formal analysis, J.L. and Y.H.; investigation, Z.D. (Zhenke Ding) and B.L.; resources, J.L. and Z.Z.; writing—original draft preparation, J.L. and E.H.; writing—review and editing, J.L. and Z.D. (Zhongliang Deng); visualization, J.L.; project administration, Z.D. (Zhongliang Deng) and Y.H. All authors have read and agreed to the published version of the manuscript.

Funding: This research was funded by the National Key Research and Development Program of China (grant number: 2022YFB3904702 and 2022YFB3904603), and the National Natural Science Foundation of China under Grants: 6220020330.

Data Availability Statement: The data that support the findings of this study are available from the corresponding author upon reasonable request.

Conflicts of Interest: The authors declare no conflict of interest.

References

1. Location-Based Services Global Market Report 2023. The Business Research Company. Available online: https://www.thebusinessresearchcompany.com/report/location-based-services-global-market-report (accessed on 15 May 2023).
2. Guo, C.; Qi, S.; Guo, W.; Deng, C.; Liu, J. Structure and performance analysis of fusion positioning system with a single 5G station and a single GNSS satellite. *Geo-Spat. Inf. Sci.* **2023**, *26*, 94–106. [CrossRef]
3. Li, X.; Shen, Z.; Li, X.; Liu, G.; Zhou, Y.; Li, S.; Lyu, H.; Zhang, Q. Continuous Decimeter-Level Positioning in Urban Environments Using Multi-Frequency GPS/BDS/Galileo PPP/INS Tightly Coupled Integration. *Remote Sens.* **2023**, *15*, 2160. [CrossRef]
4. Niu, X.; Tang, H.; Zhang, T.; Fan, J.; Liu, J. IC-GVINS: A Robust, Real-Time, INS-Centric GNSS-Visual-Inertial Navigation System. *IEEE Robot. Autom. Lett.* **2023**, *8*, 216–223. [CrossRef]
5. Wang, Y.; Song, W.; Lou, Y.; Zhang, Y.; Huang, F.; Tu, Z.; Liang, Q. Rail Vehicle Localization and Mapping With LiDAR-Vision-Inertial-GNSS Fusion. *IEEE Robot. Autom. Lett.* **2022**, *79818–9825*. [CrossRef]
6. Jiang, W.; Cao, Z.; Cai, B.; Li, B.; Wang, J. Indoor and Outdoor Seamless Positioning Method Using UWB Enhanced Multi-Sensor Tightly-Coupled Integration. *IEEE Trans. Veh. Technol.* **2021**, *70*, 10633–10645. [CrossRef]
7. Liu, Q.; Gao, C.; Shang, R.; Peng, Z.; Zhang, R.; Gan, L. Environment Perception Based Seamless Indoor and Outdoor Positioning System of Smartphone. *IEEE Sens. J.* **2022**, *22*, 17205–17215. [CrossRef]
8. Kassas, Z.Z.M.; Maaref, M.; Morales, J.J.; Khalife, J.J.; Shamei, K. Robust Vehicular Localization and Map Matching in Urban Environments Through IMU, GNSS, and Cellular Signals. *IEEE Intell. Transp. Syst. Mag.* **2020**, *12*, 36–52. [CrossRef]
9. Bai, L.; Sun, C.; Dempster, A.G.; Zhao, H.; Cheong, J.W.; Feng, W. GNSS-5G Hybrid Positioning Based on Multi-Rate Measurements Fusion and Proactive Measurement Uncertainty Prediction. *IEEE Trans. Instrum. Meas.* **2022**, *71*, 8501415. [CrossRef]

10. Yin, L.; Ni, Q.; Deng, Z. A GNSS/5G Integrated Positioning Methodology in D2D Communication Networks. *IEEE J. Sel. Areas Commun.* **2018**, *36*, 351–362. [CrossRef]
11. Ruan, Y.; Chen, L.; Zhou, X.; Liu, Z.; Liu, X.; Guo, G.; Chen, R. iPos-5G: Indoor Positioning via Commercial 5G NR CSI. *IEEE Internet Things J.* **2023**, *10*, 8718–8733. [CrossRef]
12. Liu, J.; Deng, Z.; Deng, X.; Luo, K. BDS-5G Hybrid Positioning Based on Signal Quality Assessment and Adaptive Switchover Strategy based on Measurement Uncertainty Evaluation. In Proceeedings of the 2022 IEEE 8th International Conference on Computer and Communications, Chengdu, China, 9–12 December 2022; pp. 435–440. [CrossRef]
13. Shuai, Q.; Guo, F.; Li, G.; Zhao, X.; Zhu, B.; Sun, J. A Dynamic Continuous Constrained Phase Factor Graph Optimization Method for GNSS Kinematic Precise Point Positioning. *IEEE Sens. J.* **2023**, *23*, 10739–10747. [CrossRef]
14. Li, X.; Dick, G.; Lu, C.; Ge, M.; Nilsson, T.; Ning, T.; Wickert, J.; Schuh, H. Multi-GNSS Meteorology: Real-Time Retrieving of Atmospheric Water Vapor From BeiDou, Galileo, GLONASS, and GPS Observations. *IEEE Trans. Geosci. Remote Sens.* **2015**, *53*, 6385–6393. [CrossRef]
15. Hu, G.; Xu, L.; Gao, B.; Chang, L.; Zhong, Y. Robust Unscented Kalman Filter-Based Decentralized Multisensor Information Fusion for INS/GNSS/CNS Integration in Hypersonic Vehicle Navigation. *IEEE Trans. Instrum. Meas.* **2023**, *72*, 8504011. [CrossRef]
16. Guo, Y.; Vouch, O.; Zocca, S.; Minetto, A.; Dovis, F. Enhanced EKF-Based Time Calibration for GNSS/UWB Tight Integration. *IEEE Sens. J.* **2023**, *23*, 552–566. [CrossRef]
17. Katriniok, A.; Abel, D. Adaptive EKF-Based Vehicle State Estimation With Online Assessment of Local Observability. *IEEE Trans. Control. Syst. Technol.* **2016**, *24*, 1368–1381. [CrossRef]
18. Julier, S.J.; Uhlmann, J.K. Unscented filtering and nonlinear estimation. *Proc. IEEE* **2004**, *92*, 401–422. [CrossRef]
19. Xu, Q.; Gao, Z.; Yang, C.; Lv, J. High-Accuracy Positioning in GNSS-Blocked Areas by Using the MSCKF-Based SF-RTK/IMU/Camera Tight Integration. *Remote Sens.* **2023**, *15*, 3005. [CrossRef]
20. Liu, C.; Jiang, C.; Wang, H. Variable Observability Constrained Visual-Inertial-GNSS EKF-Based Navigation. *IEEE Robot. Autom. Lett.* **2022**, *7*, 6677–6684. [CrossRef]
21. Hu, G.; Gao, S.; Zhong, Y.; Gao, B.; Subic, A. Modified federated Kalman filter for INS/GNSS/CNS integration. *Proc. Inst. Mech. Eng. G J. Aerosp. Eng.* **2016**, *230*, 30–44. [CrossRef]
22. Hajati, N.; Rezaeizadeh, A. A Wearable Pedestrian Localization and Gait Identification System Using Kalman Filtered Inertial Data. *IEEE Trans. Instrum. Meas.* **2021**, *70*, 2507908. [CrossRef]
23. der Merwe, R.V.; Wan, E.A. The square-root unscented Kalman filter for state and parameter-estimation. In Proceedings of the 2001 IEEE International Conference on Acoustics, Speech, and Signal Processing, Salt Lake City, UT, USA, 7–11 May 2001; Volume 6, pp. 3461–3464. [CrossRef]
24. Jafarzadeh, S.; Lascu, C.; Fadali, M.S. Square Root Unscented Kalman Filters for state estimation of induction motor drives. In Proceedings of the 2011 IEEE Energy Conversion Congress and Exposition, Phoenix, AZ, USA, 17–22 September 2011; pp. 75–82. [CrossRef]
25. Zhang, D.; Hao, M. Tracking Magnetic Target Based on Internative Multi-Model Square Root Unscented Kalman Filter. *IEEE Trans. Magn.* **2023**, *59*, 4000312. [CrossRef]
26. Li, K.; Chang, L.; Hu, B. A Variational Bayesian-Based Unscented Kalman Filter With Both Adaptivity and Robustness. *IEEE Sens. J.* **2016**, *16*, 6966–6976. [CrossRef]
27. Zou, X.; Li, Z.; Wang, Y.; Deng, C.; Li, Y.; Tang, W.; Fu, R.; Cui, J.; Liu, J. Multipath Error Fusion Modeling Methods for Multi-GNSS. *Remote Sens.* **2021**, *13*, 2925. [CrossRef]
28. Ma, D.; Zhao, K.; Zheng, Z.; Yu, C.; Wang, Y.; Yao, Y. Indoor Positioning With Adaptive Wavelet Denoise Enhancement and Trend Surface Analysis Based Multipath Map. *IEEE Sens. J.* **2022**, *22*, 15191–15198. [CrossRef]
29. Kim, H.; Ma, X.; Hamilton, B. Tracking low-precision clocks with time-varying drifts using Kalman filtering. *IEEE/ACM Trans. Netw.* **2012**, *20*, 257–270. [CrossRef]
30. Koivisto, M.; Costa, M.; Hakkarainen, A.; Leppanen, K.; Valkama, M. Joint 3D Positioning and Network Synchronization in 5G Ultra-Dense Networks Using UKF and EKF. In Proceedings of the 2016 IEEE Globecom Workshops (GC Wkshps), Washington, DC, USA, 4–8 December 2016; pp. 1–7. [CrossRef]
31. ETSI. *Physical Channels and Modulation*; Document TS 38.211; 3GPP: Sophia Antipolis, France, 2020.
32. Liu, J.; Gao, K.; Guo, W.; Cui, J.; Guo, C. Role, path, and vision of "5G + BDS/GNSS". *Satell. Navig.* **2020**, *1*, 23. [CrossRef]